Numerical exploration of geostrophic adjustment

Jan-Adrian Kallmyr

October 8, 2021

1 Introduction

Geostrophic adjustment is the process where an unbalanced pressure perturbation adjusts to achieve geostrophic balance. A central concept of the large-scale general circulation, we will explore geostrophic adjustment by numerically solving the shallow water equations (SWEs). In particular, we will look at the flow characteristics and energetics under a set of scenarios.

In Section 2 we present the SWEs and central analytical results, while the numerical method is described in Section 3. A few central results are shown in Section 4 and briefly discussed in Section 5, wrapping up the report.

2 Theory

The linearized shallow water equations are as follows:

$$\partial_t u - f_0 v = -g\partial_x h \tag{1}$$
$$\partial_t v + f_0 u = -g\partial_y h \tag{2}$$
$$\partial_t h + D_0(\partial_x u + \partial_y v) = 0, \tag{3}$$

where ∂_{q_i} denotes partial differentiation or ordinary differentiation given the context. u and v are the zonal and meridional velocities, respectively, while h is the sea-surface height. The planetary vorticity is f_0, while g is the gravitational acceleration, and D_0 is the depth of the system.

In this report, we will study the case of a stepwise sea surface height perturbation of $\pm h_0$

$$h_i = h_0 \begin{cases} h_0, & x > 0 \\ -h_0, & x < 0 \end{cases}, \tag{4}$$

which can be solved analytically.

2.1 Dynamics

The resulting sea surface height after geostrophic adjustment is

$$h_f = h_0 \begin{cases} -1 + \exp(-x/R), & x > 0 \\ 1 - \exp(x/R), & x < 0 \end{cases}, \tag{5}$$

where $R \equiv \sqrt{gD_0}/f_0$ is the Rossby radius of deformation, i.e. the length scale where rotational effects are important. In geostrophic balance, the meridional velocity is just $v = -\partial_x h$, giving

$$v = -\frac{gh_0}{f_0 R}\exp(-|x|/R) \tag{6}$$

for the final state.

2.2 Energetics

The total energy of a system with density ρ can be decomposed into potential and kinetic components

$$V = \frac{1}{2}\rho g\big(h^2 - D_0^2\big) \tag{7}$$
$$K = \frac{1}{2}\rho D_0\big(u^2 + v^2\big), \tag{8}$$

and the available potential energy is obtained by subtracting the constant term. For an initial height perturbation eq. 4 the resulting change in available potential and kinetic energy is

$$\Delta V = -\frac{3}{2}\rho g h_0^2 R \tag{9}$$

$$\Delta K = \frac{1}{2}\rho g h_0^2 R. \tag{10}$$

Initially, the potential energy constitutes the total energy, and so from eqs. 9 and 10 the final kinetic energy should be a 1/3 of the total energy. Likewise, the potential energy should be a 2/3 of the total energy.

3 Method

The shallow water equations (eqs. 1, 2, 3) are solved numerically in the FORTRAN programming language using finite difference schemes. An Arakawa C-grid is used for representing spatial coordinates, while the temporal integration is calculated using the leapfrog scheme. Discretization then yields

$$u_{i,j}^{n+1} = u_{i,j}^{n-1} + 2\Delta t\left(-g\frac{h_{i+1,j}^n - h_{i,j}^n}{\Delta x}\right) + \frac{f_0}{4}\left(v_{i,j}^n + v_{i+1,j}^n + v_{i+1,j-1}^n + v_{i,j-1}^n\right), \tag{11}$$

$$v_{i,j}^{n+1} = v_{i,j}^{n-1} + 2\Delta t\left(-g\frac{h_{i,j+1}^n - h_{i,j}^n}{\Delta y}\right) - \frac{f_0}{4}\left(u_{i,j}^n + u_{i,j+1}^n + u_{i-1,j+1}^n + u_{i-1,j}^n\right), \tag{12}$$

$$h_{i,j}^{n+1} = h_{i,j}^n - 2\Delta t\left(\frac{u_{i,j}^n - u_{i-1,j}^n}{\Delta x} + \frac{v_{i,j}^n - v_{i,j-1}^n}{\Delta y}\right). \tag{13}$$

The energies are calculated as follows

$$V = \frac{1}{2}\rho g \sum_i \sum_j (h_{i,j})^2 \Delta x \Delta y \tag{14}$$

$$K = \frac{1}{2}\rho \sum_i \sum_j \frac{1}{2}\left(u_{i-1,j}^2 + u_{i,j}^2 + v_{i-1,j}^2 + v_{i,j}^2\right) h_{i,j}. \tag{15}$$

Unless otherwise mentioned, the following parameter values are used

$$\begin{aligned} g &= 9.81\,\mathrm{m/s^2} \\ f_0 &= 10^4\,\mathrm{m/s^2} \\ h_0 &= 0.5\,\mathrm{m} \\ D_0 &= 4000\,\mathrm{m} \\ \rho &= 1027\,\mathrm{kg/m^3}. \end{aligned}$$

The scheme grid is specified with a domain spanning 9000km zonally and 4500km meridionally with 200 grid points each. For periodic boundaries a sponge is used spanning 50 grid points. Integration happens over 40 years where the time step is determined by a stability criterion.

The model and scripts used for analysis are found in a github repository [1].

4 Results

Figure 1 shows the initial sea surface height (solid black) and compares the adjusted height and velocity profiles between numerical (solid) and analytical (dashed) solutions. Overall, there is good agreement in shape and magnitude. There are small discrepancies close to the boundaries where the numerical solution underestimates sea surface height and meridional velocity.

[1] https://github.com/janadr/MO8004/tree/master/L1

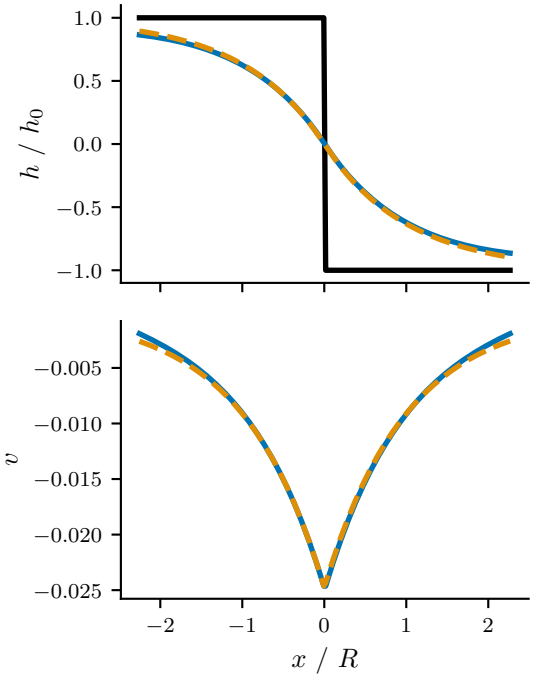

Figure 1: Upper: relative sea surface height. Lower: meridional velocity. Solid line shows numerical result, while dashed line shows analytical results. Parameters: $D_0 = 4000\,m$, $f_0 = 10^{-4}\,m/s^2$

The time evolution of relative potential (blue) and kinetic energy (orange) of the system is shown in Figure 2. The black lines marks a 1/3 and 2/3. We see that V and K fluctuate initially before converging to 2/3 for the potential energy and 1/3 for the kinetic energy, in agreement with theory.

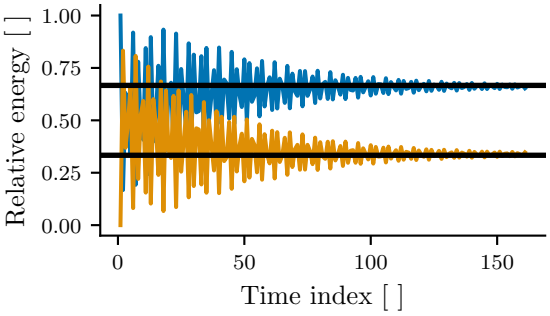

Figure 2: Relative energies where blue line shows potential energy and orange line shows kinetic energy. The horizontal black lines marks a 1/3 and 2/3. Parameters: $D_0 = 4000\,m$, $f_0 = 10^{-4}\,m/s^2$

The effect of depth is illustrated in Figure 3 where the upper plot shows a shallow basin and the lower plot a deep basin. In the shallow basin, the fraction of potential energy has increased compared with Figure 2, while the opposite is true for the kinetic energy. Additionally, the fluctuations remain around the same, larger, magnitude throughout the entire integration period. In the deep basin, the opposite case is true where the potential energy fraction has decreased and the energy converges to a value faster with smaller fluctuations compared with Figure 2.

Figure 4 shows the results of a smaller and larger planetary vorticity relative to $f_0 = 10^4\,\mathrm{m/s^2}$. A lower planetary vorticity decreases the potential energy fraction and yields faster convergence, while the opposite is the case when increasing the planetary vorticity.

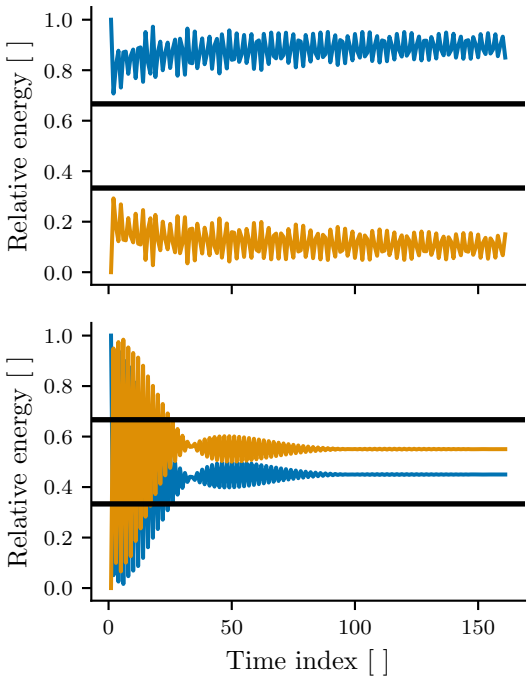

Figure 3: Relative energies where blue line shows potential energy and orange line shows kinetic energy for $D_0 = 500\,m$ (upper) and $D_0 = 10000\,m$ (lower). The horizontal black lines marks a 1/3 and 2/3. Here $f_0 = 10^{-4}\,m/s^2$

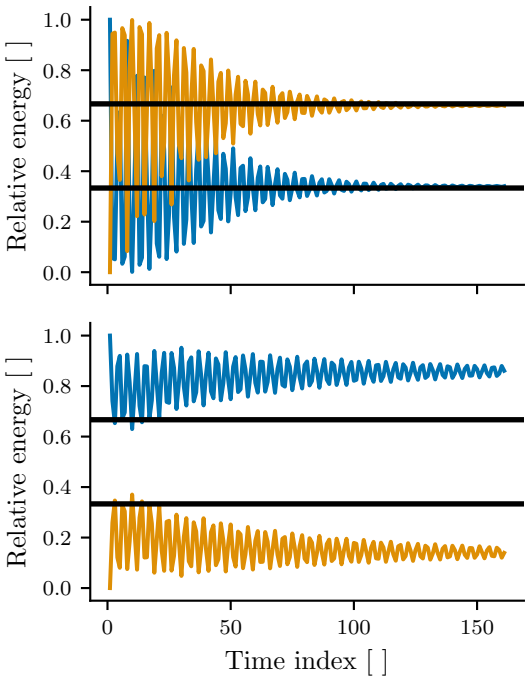

Figure 4: Relative energies where blue line shows potential energy and orange line shows kinetic energy for $f_0 = 0.5 \cdot 10^{-4}\,m/s^2$ (upper) and $f_0 = 2 \cdot 10^{-4}\,m/s^2$ (lower). The horizontal black lines marks a 1/3 and 2/3. Here $D_0 = 4000\,m$.

5 Discussion

While Figure 1 shows that there is high agreement between the numerical and analytical solutions, this result is dependent on the size of the sponge used for the periodic boundary conditions. In essence, some tuning is necessary to achieve this result, and should be taken into account. Another question may be why the final state is not that of a flat ocean surface, and this would indeed be the cause in a non-rotating system where no force can balance the pressure gradients. In a rotating system, however, this is achieved by the coriolis force.

Figures 3 and 4 illustrates that the planetary vorticity and depth have reverse effects on the result, which is not surprising due to their competing dependency in the Rossby radius of deformation. Increasing the depth or reducing the planetary vorticity will increase R, which allows for greater potential energy retention due to a larger area where the coriolis force can balance the pressure gradients.

5.1 Conclusion

In this report we have studied the dynamics and energetics of geostrophic adjustment by solving the shallow water equations numerically and analytically for a step-wise sea surface height perturbation. We found general good agreement between numerical and analytical solutions. Exploring the effect of changing the Rossby radius, we found that a larger Rossby radius tends to cause a greater fraction of the total energy to be potential energy. This was due to a overall larger contribution from rotational effects balancing pressure gradients.